

# A New Methodology for Upscaling Semi-submersible Platforms for Floating Offshore Wind Turbines

Kaylie L. Roach<sup>1</sup>, Matthew A. Lackner<sup>1</sup>, James F. Manwell<sup>1</sup>

<sup>1</sup>Mechanical Engineering, University of Massachusetts Amherst, Amherst, MA, 01003, USA

5 Correspondence to: Matthew A. Lackner (lackner@ecs.umass.edu)

**Abstract.** This paper presents a new upscaling methodology for semi-submersible floating offshore wind turbine platforms. The size and power rating of offshore wind turbines have been growing in recent years, with modern wind turbines rated at 10 - 18.4 MW in contrast with 2 - 5 MW in 2010. It is not apparent how much further wind turbines can be increased before it is unjustified. Scaling relations are a useful method for analyzing wind turbine designs, to understand the mass, load, and cost increases with size. Scaling relations currently do not exist but are needed for floating offshore platforms to understand how the technical and economic development of floating offshore wind energy may develop with increasing turbine size. In this paper, a hydrodynamic model has been developed to capture the key platform response in pitch. The hydrodynamic model is validated using OpenFAST, a high-fidelity offshore wind turbine simulation software. An upscaling methodology is then applied to two semi-submersible case studies of reference systems (5 MW OC4 and 15 MW IEA). For each case study, the platform pitch angle at rated wind turbine thrust is constrained to a specified value. The results show that platform dimensions scale to a factor of 0.75, and the platform steel mass scales to a factor of 1.5 when the wall thickness is kept constant. This study is the first to develop generalized upscaling relations that can be used for other [triangular](#) semi-submersible platforms that have three outer columns with the turbine mounted at the center of the system. This is in contrast with other studies that upscale a specific design to a larger power rating. This upscaling methodology provides new insight into trends for semi-submersible platform upscaling as turbine size increases.

## 1 Introduction

Offshore wind energy development continues to accelerate, and until now most offshore wind installations have used fixed-bottom support structures (Musial *et al.*, 2022). Offshore wind turbines are now planned for areas with deeper water depths including the coastlines of California (Speer, Keyser and Tegen, 2016; Beiter *et al.*, 2020), Japan (Yoshimoto *et al.*, 2013), and Europe (Ågotnes *et al.*, 2013), where floating offshore wind turbines (FOWTs) are needed (Jonkman, J. M., Matha, 2011; Musial *et al.*, 2016). Floating platforms have been designed and deployed in pilot projects such as the Fukushima FORWARD project in Japan (Fukushima Offshore Wind Consortium, no date; Karimirad, 2014; Kikuchi and Ishihara, 2019a), the Hywind project in Scotland (Skaare *et al.*, 2006; Karimirad, 2014; Equinor, 2021), and the WindFloat deployments in Portugal (Principle Power, no date; Karimirad, 2014; Beaubouef, 2020) and Scotland (Durakovic, 2021) with turbine power ratings of

30 2 MW - 9.5 MW, while others are planned for the U.S. in California (California Energy Commission, 2021; Conversation, 2021) and Maine (The University of Maine, 2021).

Offshore wind turbine size and capacity have been growing rapidly over the past ten years as well. Modern offshore wind turbines designed by General Electric, Siemens Gamesa, and Vestas have ratings of 10 - 18 MW with blade diameters exceeding 200 m (Siemens Gamesa, 2020; GE Renewable Energy, 2023; Vestas, 2023). GE has only recently announced their  
35 18 MW turbine design (Buljan, 2023). In contrast, in 2010 offshore turbines had power ratings between 2 - 5 MW and blade diameters were 75 - 125 m (Musial *et al.*, 2022). Even larger designs are likely to be developed in the future, with researchers even investigating a 50 MW turbine (Yao *et al.*, 2021).

While the industry is clearly trending towards larger wind turbines, the classical “cubed-square” law dictates that the per MW capital cost of a wind turbine increases with turbine size due to the mass increasing more quickly than the rated power  
40 (Manwell, McGowan and Rogers, 2009). However, looking at data of historic wind turbines, the cost does not scale with the mass because of technological innovations over time. Also, the industry trend towards larger offshore wind turbines minimizes the number of installed units in a wind farm for a given total capacity, which is motivated by the large per unit cost (including the foundation, installation, electrical interconnection, and maintenance visits at sea). Offshore wind levelized cost of energy (LCOE) is still about twice as much as onshore wind on average, but as turbine size has increased, LCOE has decreased  
45 significantly over time (Thresher, Robinson and Veers, 2008; Beiter *et al.*, 2016). As offshore wind energy development continues, it is important to understand if even larger turbines can continue to reduce the LCOE of offshore wind farms, or if there is an upper limit to the cost effectiveness and practicality of upscaling.

The process of evaluating a wind turbine design with increasing scale is referred to as “upscaling.” Classical upscaling methods can be used to project the power, size, mass, forces, moments, costs, and other properties of an upscaled turbine based on a  
50 turbine of a smaller size (Manwell, McGowan and Rogers, 2009). Upscaling methods are discussed further in Section 2. As wind turbines are rapidly increasing in power rating, research is needed to understand how the design characteristics of FOWT platforms, including the physical dimensions, mass, cost, and dynamic behavior, change with respect to the increased turbine size.

This paper aims to model and analyze semi-submersible FOWT platform design characteristics and system dynamics to  
55 provide insight into technology development of FOWT systems with larger power ratings. The objective is to develop general scaling trends, which characterize the mass, dimensions, and dynamics of the semi-submersible FOWT platform subject to constraints on the system stability as a turbine is upscaled. To achieve this objective, a new upscaling methodology for floating platforms is developed based on a hydrodynamic model that captures the key platform responses in pitch. The hydrodynamic model is validated using OpenFAST, a high-fidelity offshore wind turbine simulation software (Jonkman, 2019; National  
60 Renewable Energy Laboratory, 2020). The methodology is then applied using two semi-submersible case studies, in which the platform pitch angle at rated wind turbine thrust is constrained to a constant value. Other researchers have upscaled specific semi-submersible platforms (George, 2014; Leimeister *et al.*, 2016; Ju *et al.*, 2020; Kikuchi and Ishihara, 2020). This study is the first to develop generalized upscaling relations for triangular semi-submersible FOWT platforms with three outer columns

and a centrally mounted turbine. Ideally, this research would also be conducted with other types of semi-submersible designs, as well as other FOWT designs (spar, tension leg platform). These upscaling relations can provide new insight into design trends for three-column triangular semi-submersible platforms as turbine size increases. Additionally, the paper identifies key underlying physics behind the semi-submersible upscaling relations.

This paper is organized as follows: Section 2 provides a review of literature. Section 3 describes the methods used in this research study, including the hydrodynamic modeling of floating offshore platforms, the semi-submersible case studies, the model validation, and upscaling methodology. Section 4 presents the upscaling results, as well as a new analytical model for FOWT upscaling and parameter sensitivity studies. Finally, Section 5 summarizes the research findings and future work.

## 2 Background

Classical upscaling relations have been developed for a wind turbine with geometric and aerodynamic similarity (Manwell, McGowan and Rogers, 2009; Ashuri, 2012; Sieros *et al.*, 2012). The general form of the scaling relations is shown in Eq. (1).

The upscaled parameter (denoted with subscript 2) depends on the ratio of the upscaled to the original rotor radius ( $R$ ), original parameter size (denoted with subscript 1), and the scale dependence power  $\alpha$ . Table 1 shows the scaling relations for power, forces, weight, moments, stresses, and resonances for a wind turbine (Manwell, McGowan and Rogers, 2009).

$$\frac{Parameter_1}{Parameter_2} = \left( \frac{Radius_1}{Radius_2} \right)^\alpha = R^\alpha \quad (1)$$

Table 1: Classical Scaling Relations (Manwell, McGowan and Rogers, 2009)

Quantity	Symbol	Relation	Scale dependence
<b>Power, forces, and moments</b>			
Power	$P$	$P_1/P_2 = (R_1/R_2)^2$	$\sim R^2$
Torque	$Q$	$Q_1/Q_2 = (R_1/R_2)^3$	$\sim R^3$
Thrust	$T$	$T_1/T_2 = (R_1/R_2)^2$	$\sim R^2$
Rotational speed	$\Omega$	$\Omega_1/\Omega_2 = (R_1/R_2)^1$	$\sim R^{-1}$
Weight	$W$	$W_1/W_2 = (R_1/R_2)^3$	$\sim R^3$
Aerodynamic moments	$M_A$	$M_{A,1}/M_{A,2} = (R_1/R_2)^3$	$\sim R^3$
Centrifugal forces	$F_c$	$F_{c,1}/F_{c,2} = (R_1/R_2)^2$	$\sim R^2$
<b>Stresses</b>			
Gravitational	$\sigma_g$	$\sigma_{g,1}/\sigma_{g,2} = (R_1/R_2)^1$	$\sim R^1$
Aerodynamic	$\sigma_A$	$\sigma_{A,1}/\sigma_{A,2} = (R_1/R_2)^0 = 1$	$\sim R^0$
Centrifugal	$\sigma_c$	$\sigma_{c,1}/\sigma_{c,2} = (R_1/R_2)^0 = 1$	$\sim R^0$
<b>Resonances</b>			
Natural frequency	$\omega$	$\omega_{n,1}/\omega_{n,2} = (R_1/R_2)^1$	$\sim R^{-1}$
Excitation	$\Omega/\omega$	$(\Omega_1/\omega_{n,1})/(\Omega_2/\omega_{n,2}) = (R_1/R_2)^0 = 1$	$\sim R^0$
Note: $R$ , radius			

Formatted: Font: Italic

Formatted: Font: Italic

The rotor power is related to the scaling factor squared ( $R^2$ ), because it is proportional to rotor swept area. The weight of the wind turbine rotor increases with  $R^3$  because of the volumetric upscaling with geometric similarity (Manwell, McGowan and Rogers, 2009). This “square-cube law” therefore implies that mass will increase more quickly than rated power as a turbine is

85 upscaled, which would seem to argue against increasing the turbine size. The aerodynamic stresses are independent of rotor size, while stresses due to the blade weight increase in proportion to the rotor radius and may eventually drive the design loads for an upscaled rotor.

Historical data from wind turbines of different sizes can also be used to understand upscaling trends. For example, historical data indicates that the rotor mass has increased to the power of between 2 and 2.5, not the cubic power of the square-cube law (Figure 1) (Jamieson, 2018). This smaller value for the scaling exponent is primarily due to technological innovation, such as new materials and improved manufacturing, in newer designs that are usually larger in size (Jamieson, 2018; Shields *et al.*, 2021).

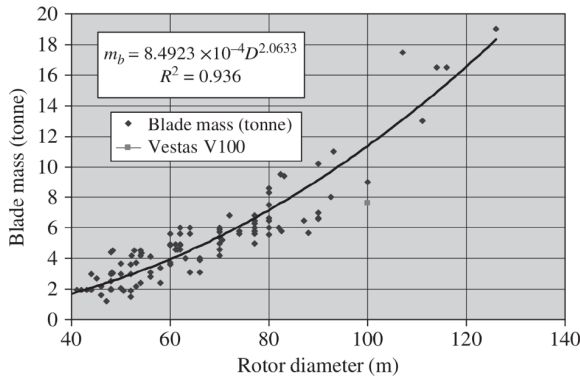


Figure 1: Blade Mass Scaling Based on Data (Jamieson, 2018)

As wind turbines become larger, the mass and aerodynamic forces increase as well, and so the floating platform that supports the turbine must grow to ensure a stable system. Several researchers have studied floating platform upscaling for a specific case study (George, 2014; Leimeister *et al.*, 2016; Ju *et al.*, 2020; Kikuchi and Ishihara, 2020), including multiple studies of semi-submersible FOWT platforms (George, 2014; Leimeister *et al.*, 2016; Kikuchi and Ishihara, 2019a). George (George, 2014) upscales the 5 MW OC4 semi-submersible FOWT to 7.5 MW and 10 MW (Robertson, A., Jonkman, J., Masciola, M., Song, 2014). Leimeister *et al.* (Leimeister, 2016) also upscale the 5 MW OC4 reference FOWT platform to 7.5 MW and 10 MW. Kikuchi and Ishihara (Kikuchi and Ishihara, 2019a) upscale the 2 MW Fukushima Forward semi-submersible FOWT to 5 MW and 10 MW (Fukushima Offshore Wind Consortium, no date). Leimeister *et al.* (Leimeister *et al.*, 2016) upscale all platform parameters, and then check the static pitch of the turbine at rated wind speed to iteratively adjust parameters as needed. Both George (George, 2014) and Kikuchi and Ishihara (Kikuchi and Ishihara, 2019b) keep the draft constant due to constraints of harbor depth. The other parameters are scaled, and the static pitch is evaluated; the design is iterated until the static pitch matches the original design. Each of these three studies finds that it is technically and economically feasible to upscale the

semi-submersible system. Leimeister et al. (Leimeister *et al.*, 2016) find that the upscaled system had to also be designed for the heave natural period, and recommends having different scaling factors for different parts of the platform.

Wu and Kim (Wu and Kim, 2021) have developed a methodology for upscaling a FOWT turbine and semi-submersible platform by using the 5 MW OC4 and 15 MW IEA semi-submersible systems. The central column diameter is set to be equal  
110 to the tower diameter and a guess is made for the scale factor, which is applied to the column radius and distance between columns. The buoyancy is calculated, and the ballast mass is set to match the total weight with the buoyancy. The scaling factor for the distance between columns and column radius is adjusted iteratively until the desired platform pitch angle is reached. Additionally, the same methodology is followed while keeping the column radius constant and only increasing the distance between the columns.

115 When upscaling a FOWT, specific load cases are typically used to constrain the design and ensure acceptable stability and dynamics. Load cases at rated wind speed often govern the extreme loads of FOWT systems (George, 2014; Leimeister *et al.*, 2016; Kikuchi and Ishihara, 2019a; Wu and Kim, 2021; Souza and Bachynski-Polić, 2022). Silva de Souza and Bachynski-Polic (Souza and Bachynski-Polić, 2022) study the behavior of a large spar FOWT and find that the extreme loads are governed by the rated wind speed cases rather than the extreme wind and sea state cases.

## 120 **3 Methodology**

In this section, a hydrodynamic model for FOWT platforms is presented, which can be used to assess the static stability and natural period of a platform based on the geometry. The hydrodynamic model is validated using OpenFAST. This model is then used in two upscaling case studies, which are carried out for two semi-submersible platforms.

### **3.1 Hydrodynamic Modeling of Floating Platforms**

125 FOWT platforms stabilize the offshore wind turbine system, allowing the turbine to produce power while floating in the water.

[Figure 2](#) ~~Figure-2~~ shows the three primary FOWT platform types: spar, semi-submersible, and tension leg platform (Speer, Keyser and Tegen, 2016). Floating platforms can be stabilized by ballast, buoyancy, moorings, or a combination (Wang *et al.*, 2010; Karimirad, 2014; Thiagarajan and Dagher, 2014; Speer, Keyser and Tegen, 2016). This study focuses on semi-submersible FOWT platforms, which is primarily stabilized by the large waterplane area of the offset columns, with a wider  
130 spread adding more stability.

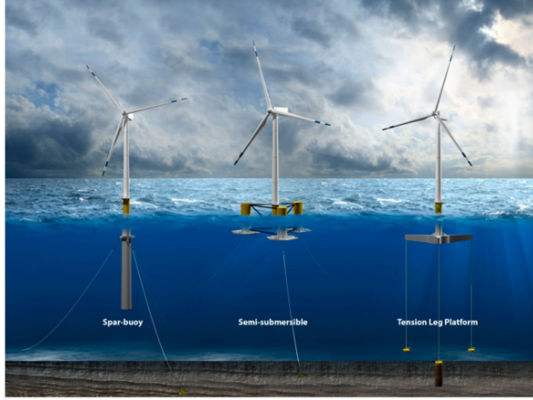


Figure 2: Types of Floating Offshore Wind Platforms (illustration by Joshua Bauer, NREL) (Speer, Keyser and Tegen, 2016)

OpenFAST is a simulation tool developed by the National Renewable Energy Laboratory (NREL) used to evaluate offshore wind turbines (Jonkman, 2019; National Renewable Energy Laboratory, 2020). The aerodynamics, hydrodynamics, elastodynamics, and system controls are all incorporated into a coupled simulation. OpenFAST is widely used in academia and industry for wind turbine modeling and simulation.

The stability of a FOWT can be characterized using the hydrodynamic loading and response. Eq. (2), known as the Cummins equation, is the equation of motion for an offshore platform in water with six degrees of freedom (TU Delft, 2006; Jonkman, 2007; Duarte, Sarmento and Jonkman, 2014).  $M_{ii}$  is the mass or mass moment of inertia term,  $A_{ii}$  is the added mass coefficient term,  $K_{ii}$  is the retardation matrix, and  $C_{ii}$  is the stiffness matrix. The platform acceleration, velocity, and displacements are represented by  $\dot{q}^{tot}$ ,  $\dot{q}^{tot}$ , and  $q^{tot}$  respectively,  $F_i^{waves}$  is the external wave loading,  $F_i^{rotor}$  is the force of the wind turbine acting on the floating platform, and  $h_i$  is the moment arm of  $F_i^{rotor}$  for rotational platform degrees of freedom. The six degrees of freedom are labeled with  $i = 1, 2, \dots, 6$  and correspond to (surge, sway, heave, roll, pitch, yaw). Figure 3 shows the FOWT coordinate system (Sebastian and Lackner, 2012).

$$(M_{ii} + A_{ii})\ddot{q}^{tot} + \int_0^T K_{ii}(t - \tau)\dot{q}^{tot}(\tau) d\tau + C_{ii}\dot{q}^{tot} = F_i^{waves} + F_i^{rotor} * h_i \quad (2)$$

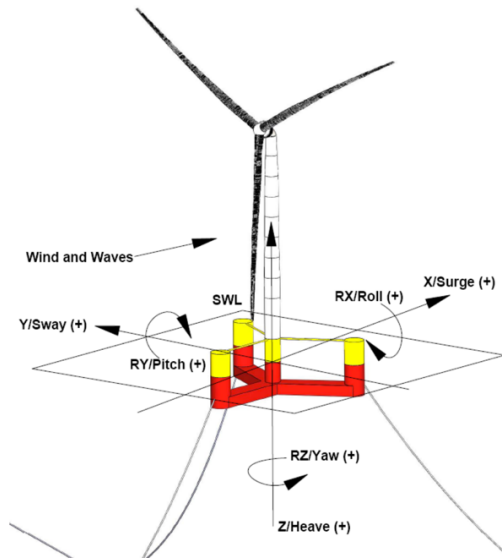


Figure 3: FOWT Platform Degrees of Freedom on IEA 15 MW System (Allen *et al.*, 2020)

When the platform is in static equilibrium, the acceleration and velocity terms are zero; ignoring the wave forcing leaves only the hydrostatic stiffness term balancing the aerodynamic forces and moments  $C_{ii}q^{tot} = F_i^{rotor} * h_i$ . The stiffness term,  $C_{ii}$  is  
 150 comprised of both platform stiffness,  $C_{ii}^{hydrostatics}$ , and mooring line stiffness,  $C_{ii}^{lines}$ . This study focuses on the stiffness contributions from the platform rather than the mooring lines. The mooring lines provide a restoring force in the surge (1,1), sway (2,2), and yaw (6,6) degrees of freedom, but this study focuses primarily on the pitch (5,5) degree of freedom (Delhommeau, 1993). For the pitch degree of freedom,  $h_i$  is the distance from the system center of mass to the rotor hub.  
 In OpenFAST, the hydrostatic stiffness matrix,  $C_{ii}^{hydrostatics}$ , is defined using only the waterplane area and center of buoyancy;  
 155 the center of mass is calculated separately (Jonkman, 2007). However, the hydrostatic stiffness of a platform has contributions from both gravity and buoyancy in this study, which is traditional in the field of naval architecture, and is used in the pitch angle Eq. (4) below. Eq. (3) shows the hydrostatic stiffness matrix,  $C_{ii}^{hydrostatics}$ , for an offshore platform (Delhommeau, 1993). The displaced volume is  $V_{disp}$ , the center of buoyancy is  $B$ , and the center of mass is  $CM$ . The matrix is symmetric, and has nonzero components including (3,3), (4,4), (5,5), (3,4), (3,5), and (4,5), corresponding to the heave (3,3), roll (4,4), and  
 160 pitch (5,5) degrees of freedom.

$$C_{ij}^{hydrostatic} = \begin{bmatrix} 0 & 0 & 0 & 0 & 0 & 0 \\ 0 & 0 & 0 & 0 & 0 & 0 \\ 0 & 0 & C_{33} & C_{34} & C_{35} & 0 \\ 0 & 0 & C_{43} & C_{44} & C_{45} & 0 \\ 0 & 0 & C_{53} & C_{54} & C_{55} & 0 \\ 0 & 0 & 0 & 0 & 0 & 0 \end{bmatrix} \quad (3)$$

with:

$$C_{33} = \rho g W_0$$

$$165 \quad C_{44} = \rho g \iint_{W_0} Y^2 dW + \rho g V_{disp} (B - CM)$$

$$C_{55} = \rho g \iint_{W_0} X^2 dW + \rho g V_{disp} (B - CM)$$

$$C_{34} = C_{43} = \rho g \iint_{W_0} Y dW$$

$$C_{35} = C_{53} = -\rho g \iint_{W_0} X dW$$

$$C_{45} = C_{54} = -\rho g \iint_{W_0} XY dW$$

170 The platform has a non-zero mean pitch angle during normal operation due to aerodynamic forces. The static platform pitch angle at rated thrust (maximum thrust condition) can be calculated using Eq. (4) based on the thrust at rated wind speed,  $F_5^{rotor}$ , height from rotor nacelle assembly to the waterline,  $h_{hub}$ , and pitch stiffness  $C_{55}^{hydrostatics}$ .

$$\theta_p = \frac{F_5^{rotor} h_{hub} r_{ts}^{rotor} (h_{tower})}{C_{55}^{hydrostatics}} \quad (4)$$

175 The natural period for offshore structures with catenary moorings is typically over 100 s in surge, sway, and yaw, and over 20 s in heave, roll, and pitch (Det Norske Veritas Germanischer Lloyd, 2017). The natural period of the system is designed to be outside the dominant period range of the wave climate, so that the structure is not excited by the ocean waves. The natural period for a moored structure is approximately given by Eq. (5) (Det Norske Veritas Germanischer Lloyd, 2017; Kikuchi and Ishihara, 2020). This research includes hydrostatic stiffness, but not mooring line stiffness; a mooring line sensitivity study is presented in Section 4.6.1.

$$180 \quad T_i = 2\pi \sqrt{\frac{M_{ii} + A_{ii}(M_{zz} + A_{zz})}{C_{ii}^{hydrostatics} + C_{ii}^{lines} (C_{zz}^{hydrostatics} + C_{zz}^{lines})}} \quad (5)$$

Formatted: Font: Italic

Formatted: Font: Italic

Formatted: Font: Italic

Formatted: Font: Italic

Formatted: Font: Italic

Formatted: Font: Italic



### 3.2 Case Study Semi-submersible Models

Two semi-submersible platforms are used as case studies for upscaling. Reference FOWT systems developed by both NREL and the International Energy Agency (IEA) are selected: the OC4 5 MW semi-submersible (Robertson, A., Jonkman, J., Masciola, M., Song, 2014) and the IEA 15 MW semi-submersible (Allen *et al.*, 2020). In Section 3.4, an upscaling methodology for the floating platforms is presented, which is then applied to these two case studies.

#### 3.2.1 OC4 Semi-submersible Model

The 5 MW OC4 is a semi-submersible platform with three outer columns, and one central column below the tower, connected with cross braces (Figure 4). The properties are shown in Table 2. Sea water ballast is used within the three outer columns, with the heave plates filled and the upper part of the column partially filled. The 5 MW reference turbine has a 63 m radius with a rated wind speed of 11.4 m/s. The turbine properties are summarized in Table 3.

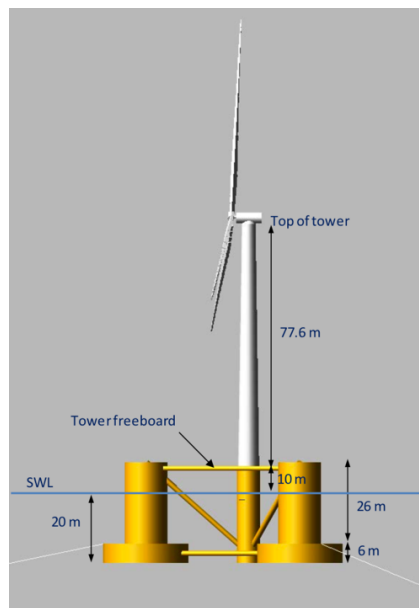


Figure 44: OC4 Platform Dimensions (Robertson, A., Jonkman, J., Masciola, M., Song, 2014)

Formatted: English (UK)

Formatted: French

Formatted: French

Field Code Changed

Field Code Changed

Formatted: Font: Bold, French



**Table 4: Rotor Radius of Upscaled OC4 Turbines**

Power rating (MW)	10	15	20
Rotor radius (m)	89	109	126
Hub height (m)	119	139	156
	20	126	156

Formatted: Font: Cambria Math, 9 pt

Formatted: Font: Cambria Math, 9 pt

### 215 3.2.2 IEA Semi-submersible Model

The IEA 15 MW turbine was designed with both a semi-submersible platform and also a monopile (Allen *et al.*, 2020; Gaertner *et al.*, 2020). The 15 MW IEA semi-submersible platform has three outer columns and one central column to support the turbine (Figure 3). The 20 m draft is the same as the OC4 semi-submersible. Semi-submersible platforms have a relatively shallow draft compared to a spar platform, and this is prioritized for the 15 MW design which has a 20 meter draft. One noticeable difference between the OC4 and IEA designs is the pontoons between the three outer columns, instead of heave plates. The IEA 15 MW semi-submersible platform properties are shown in Table 5.

**Table 5: IEA 15 MW Semi-submersible Platform Properties (Allen *et al.*, 2020)**

Draft	20	m
Freeboard	15	m
Distance between columns ( $Dist_{co}$ )	89.63	m
Radius of Upper Columns ( $Rad_{co}$ )	6.25	m
Pontoon height ( $H_{poo}$ )	7	m
Platform mass including ballast	1.78E+07	kg
Seawater ballast mass	1.13E+07	kg
Iron-ore ballast mass	4.80E+06	kg
$\Delta CM_{platform}$ about $CM_{platform}$ in pitch	1.251E+10	kg-m <sup>2</sup>
$CM_{platform}$ below waterline	-14.94	m

Formatted: Font: Cambria Math, 9 pt

Formatted: Font: Cambria Math, 9 pt

Formatted: Font: Cambria Math, 9 pt

Formatted: Font: Cambria Math, 9 pt, Italic

Formatted: Font: Cambria Math, 9 pt

Formatted: Font: Cambria Math, 9 pt

Formatted: Font: Cambria Math, 9 pt

Formatted: Font: Cambria Math, 9 pt, Italic

Formatted: Font: Cambria Math, 9 pt

Formatted: Font: Cambria Math, 9 pt

Formatted: Font: Cambria Math, 9 pt, Italic

Formatted: Font: Cambria Math, 9 pt

Formatted: Font: Cambria Math, 9 pt

Formatted: Font: Cambria Math, 9 pt

Formatted: Font: Cambria Math, 9 pt, Italic

Formatted: Font: Cambria Math, 9 pt

Formatted: Font: Cambria Math, 9 pt, Italic

Formatted: Font: Cambria Math, 9 pt

Formatted: Font: Cambria Math, 9 pt

Formatted: Font: Cambria Math, 9 pt, Italic

Formatted: Font: Cambria Math, 9 pt

Formatted: Font: Cambria Math, 9 pt

Formatted: Font: Cambria Math, 9 pt

Formatted: Font: Cambria Math, 9 pt

Formatted: Font: Cambria Math, 9 pt

Formatted: Font: Cambria Math, 9 pt

Formatted: Font: Cambria Math, 9 pt

Formatted: Font: Cambria Math, 9 pt

**Table 6: 15 MW Reference Turbine Properties (Gaertner *et al.*, 2020)**

Rated power	15	MW
Rotor radius	120	m
Hub height	150	m
Rated wind speed	10.59	m/s
Rotor mass	3.85E+05	kg
Nacelle mass	6.31E+05	kg
Tower mass	1.26E+06	kg

Formatted: Font: Cambria Math, 9 pt

225

$Sp$	332	W/m <sup>2</sup>
------	-----	------------------

Formatted: Font: Cambria Math, 9 pt, Italic

Formatted: Font: Cambria Math, 9 pt

Table 7: Rotor Radius of Upscaled IEA Turbines

Power rating (MW)	20 Rotor radius (m)	25 Hub height (m)	30
Rotor radius (m) 20	138	15568	170
Hub height (m) 25	16855	185	200
30	170	200	

Formatted: Font: Cambria Math, 9 pt

Formatted: Font: Cambria Math, 9 pt

230

The 15 MW reference turbine has a rotor radius of 120 m and a rated wind speed of 10.59 m/s. The turbine has a lower specific power of 332 W/m<sup>2</sup> compared to the 5 MW reference turbine (401 W/m<sup>2</sup>) because of the lower rated wind speed. The turbine properties are summarized in [Table 6](#). The 15 MW IEA semi-submersible wind turbine is upscaled to 20 MW, 25 MW, and 30 MW. The rotor diameters of the three upscaled turbines are shown in [Table 7](#). Again, the tower mass is upscaled by a factor of 2 and the [rotor nacelle assembly \(RNA\)](#) mass is upscaled by a factor of 2.2. The hub height is calculated assuming that there is a 30 m gap between the bottom of the rotor plane and the waterline.

### 3.3 Verification of the Hydrodynamic Model for Case Study Turbines

235

The hydrodynamic model presented in [Section 3.1](#) is validated by simulating the two case study reference turbines in OpenFAST (Jonkman and Buhl, 2005; National Renewable Energy Laboratory, 2020). OpenFAST is used to calculate the static platform pitch under steady, rated wind speed and to calculate the pitch natural period ( $T_n$ ) of the system. The OC4 semi-submersible platform result for platform pitch angle is shown in [Figure 5](#), which is estimated as 3.26°. The platform pitch value calculated using the presented hydrodynamic model Eq. (4) is 3.55°. Both platform pitch angles are relative to the waterline. The 9% error is acceptable for the purpose of setting the platform pitch angle for upscaling, especially since the proposed model is much less computationally expensive than OpenFAST.

240

245

The natural period of the OC4 semi-submersible is evaluated in OpenFAST by using a free decay test ([Figure 6](#)), with an initial platform pitch angle of 8°. Based on this test, the  $T_{n, \text{natural period}}$  of the system is 25.5 s. The published  $T_{n, \text{natural period}}$  is 27.0 s (Robertson, A., Jonkman, J., Masciola, M., Song, 2014). The pitch  $T_{n, \text{natural period}}$  of the system calculated using the hydrodynamic model Eq. (5) is 24.2 s, with 10% error relative to the published value and 5% error relative to the  $T_{n, \text{natural period}}$  found using OpenFAST. The error is likely due to second order effects in OpenFAST that are not captured in the hydrodynamic model.

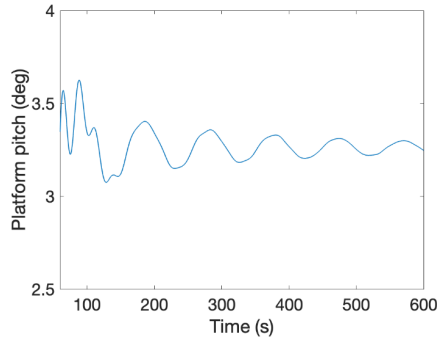


Figure 5: OC4 Platform Pitch Angle at Rated Wind Speed Using OpenFAST

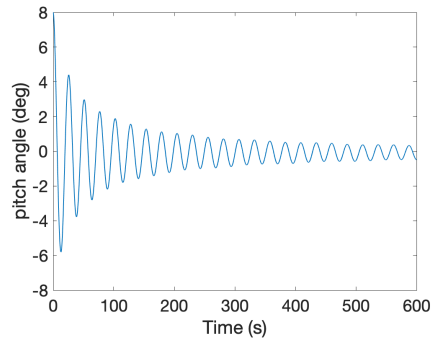


Figure 6: Free Decay of OC4 Semi-submersible Using OpenFAST

250

OpenFAST is also used to simulate the 15 MW IEA wind turbine with the semi-submersible platform. The static platform pitch angle is estimated as  $3.6^\circ$  at steady, rated wind speed (Figure 7). The platform pitch angle found using the hydrodynamic model Eq. (4) is  $4.9^\circ$ . This 36% error in static pitch angle as compared with the OpenFAST model may be due to limitations in what is known about the IEA 15 MW system. For instance, the system center of mass and moment of inertia is published for the 5 MW OC4 system, but not published for the IEA 15 MW system. The platform pitch angle from the hydrodynamic model can be used as a relative rather than absolute pitch angle in order to constrain the upscaled turbine platform pitch angle. The pitch  $T_n$  natural period from the OpenFAST free decay test (Figure 8) is estimated as 27.7 s, the published value is 29.5 s, and the result from the hydrodynamic model is 28.6 s. The model has a 3% error relative to the OpenFAST results and a 3% error relative to the published value. The verification results are summarized in Table 8.

The purpose of this verification was to confirm that the calculations were similar to both published values as well as OpenFAST simulations. The model could be further verified with other simulation software or with data from FOWT pilot projects, but further validation is outside the scope of this paper.

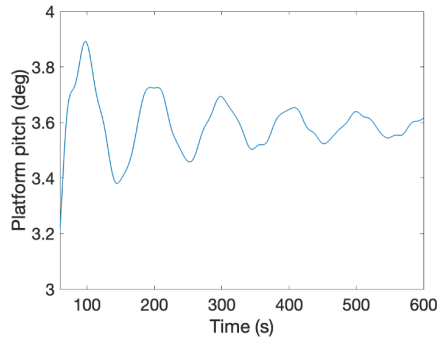


Figure 7: IEA 15 MW Platform Pitch Angle at Rated Wind Speed Using OpenFAST

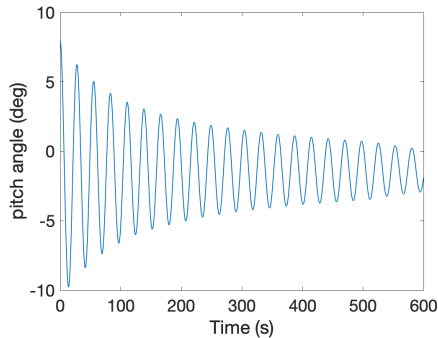


Figure 8: Free Decay of IEA 15 MW Using OpenFAST

Table 8: Model Verification

		OC4 5MW	IEA 15MW
Platform pitch	Hydrodynamic model	3.94	4.90
angle (deg)	OpenFAST	3.26	3.60
Pitch natural	Hydrodynamic model	24.2	28.6
period (s)	OpenFAST	25.5	27.7

- Formatted: Font: Cambria Math, 9 pt
- Formatted: Font: Cambria Math, 9 pt, Not Bold
- Formatted: Font: Cambria Math, 9 pt, Not Bold
- Formatted Table
- Formatted: Font: Cambria Math, 9 pt
- Formatted: Font: Cambria Math, 9 pt, Not Bold
- Formatted: Font: Cambria Math, 9 pt

	Published	27.0	29.5
--	-----------	------	------

### 270 3.4 Upscaling Methodology

The semi-submersible platforms are upscaled by first upscaling the turbine to a higher power rating, and then using the following methodology for the platforms:

1. Linearly increase the platform dimensions, specifically the column radii and spacing, with a scaling constant  $\alpha$  Eq. (1).
- 275 2. Use the hydrodynamic model to find the static pitch angle at rated wind speed Eq. (4) and natural period Eq. (5).
3. Continue to increase the platform dimensions with the scaling constant  $\alpha$  until the upscaled static pitch angle is equivalent to the static pitch angle of the original case study.

This method is effectively a root-finding problem to determine the value of  $\alpha$  that results in equal rated platform pitch angles for the baseline and upscaled turbines. While it may be possible to solve for a single alpha value analytically, the root-finding approach was selected because it allows us to see trends ~~for~~in the platform behavior. We can clearly see how the upscaling value of  $\alpha$  would-results in a more conservative or less conservative design. The platform dimensions are upscaled uniformly with the scaling constant  $\alpha$  in Eq. (1), which is increased from 0 to 2 in increments of 0.005. The wall thickness and clearance between the blade tip and the waterline are kept constant during upscaling. The 30 m clearance between the rotor and the  
 285 waterline was chosen because the literature and industry trends show that the 30 m clearance is typical for offshore wind turbines to date (Robertson, A., Jonkman, J., Masciola, M., Song, 2014; Allen *et al.*, 2020). The system mass, buoyancy, ballast mass, center of buoyancy, center of mass, static pitch stiffness, static pitch angle, and pitch natural period are calculated for each turbine size (10 - 30 MW) and  $\alpha$  scaling constant. In this paper the  $CM_{system}$  includes the total system center of mass, including the turbine, tower, and platform. In contrast, the  $CM_{platform}$  is used for the platform center of mass, excluding the turbine and tower. The platform pitch stiffness is calculated using Eq. (7), which comes from  $C_{55}$  in Eq. (3). The distance from  
 290 one outer columns to another is  $Dist_{cc}$ .

$$C_{55} = \rho g \left( V_{disp}(B - CM_{system}) + \frac{\pi}{4}(Rad_{cent})^4 + \frac{3\pi}{4}(Rad_{col})^4 + 2\pi(Rad_{col})^2 \left( \frac{Dist_{cc}}{2} \right)^2 \right) \quad (7)$$

The platform is upscaled until the platform pitch angle at rated wind speed matches the initial design platform pitch angle in Eq. (4). The pitch  ~~$T_n$  natural period~~ is calculated using Eq. (8) (derived from Eq. (5)) to ensure that it is not in the predominant  
 295 wave period range. The pitch  $T_n$  of a semi-submersible platform should always be above 20 s (Det Norske Veritas Germanischer Lloyd, 2017). The added mass coefficient  $c_A$  comes from the documentation for each semi-submersible case study (Robertson, A., Jonkman, J., Masciola, M., Song, 2014; Allen *et al.*, 2020). The moment of inertia of the system is  $I_{system}$  and the moment of inertia of the platform is  $I_{platform}$ .

Field Code Changed

Formatted: French

Formatted: French

$$T_{55} = \sqrt{\frac{I_{system} + CA_{platform}(\alpha)(I_{platform})}{C_{55}}} \quad (8)$$

### 3.4.1 OC4 Semi-submersible Upscaling Method

The OC4 semi-submersible turbine is upscaled from 5 MW to 10 MW, 15 MW, and 20 MW. The OC4 platform draft is kept at a constant 20 m and the wall thickness is kept constant at 6 cm. The ballast is sea water with a density of 1,025 kg/m<sup>3</sup>. The center of mass of the entire OC4 system is -10 m, while the center of mass ( $CM_{platform}$ ) of the OC4 platform is -13.46 m.

The platform displaced volume is set using Eq. (9). The system buoyancy is equal to the mass of the displaced water. The platform steel mass is calculated with the upscaled dimensions, and the ballast mass is the difference between the buoyancy and the steel mass. The radius of the outer columns at the waterline is  $Rad_{col}$ , the height of the heave plate on the lower part of the columns is  $H_{hp}$ , the radius of the heave plate is  $Rad_{hp}$ , and the radius of the central column below the tower is  $Rad_{center}$ .

$$V_{disp} = 3(\pi(Rad_{col})^2(draft - H_{hp}) + \pi(Rad_{hp})^2 H_{hp}) + \pi(Rad_{center})^2 draft \quad (9)$$

### 3.4.2 IEA Semi-submersible Upscaling Method

The IEA 15 MW turbine is upscaled to 20 MW, 25 MW, and 30 MW. Since both the 15 MW IEA and the 5 MW OC4 had an equivalent draft of 20 m, the OC4 platform upscaling kept the draft constant. However, the IEA platform draft is increased with  $\alpha$  for the larger turbines. The upscaled IEA platform wall thickness is kept at a constant 4.5 cm. The IEA platform has sea water ballast filling the pontoons and an iron-ore ballast partially filling the columns. The iron-ore ballast density is estimated to be 4,300 kg/m<sup>3</sup>. The center of buoyancy, center of mass of the platform, and center of mass of the entire system are calculated. The  $CM_{platform}$  of the IEA 15 MW platform is -15 m while the total  $CM_{system}$  of the system is -2.8 m.

The displaced volume is calculated using Eq. (10). The platform steel mass, buoyancy mass, and ballast mass are calculated. The sea water ballast fills up the pontoon inner volume. The remaining ballast mass partially fills the three outer columns with iron-ore. The column radius for this type of semi-submersible platform is  $Rad_{col}$  and the radius of the central column is  $Rad_{center}$ , the pontoon length, width, and height are  $L_{pon}$ ,  $W_{pon}$ , and  $H_{pon}$  respectively.

$$V_{disp} = 3(\pi(Rad_{col})^2 draft + L_{pon} * W_{pon} * H_{pon}) + \pi(Rad_{center})^2 draft \quad (10)$$

## 4 Results and Discussion

In this section, the case study results using the methodology presented in Section 3 are analyzed. First, the results are given for the OC4 platform upscaling results (4.1) and the IEA platform upscaling results (4.2). The results from both case studies are compared with each other (4.3), and then compared with similar studies from the literature (4.4). An analytical model for



semi-submersible platform upscaling is shown as a comparison to the iterative upscaling results (4.5), and the sensitivity studies are presented (4.6).

#### 330 4.1 OC4 Platform Upscaling Results

The platform pitch angle at rated thrust is plotted for each upscaling factor value in Figure 9. As the  $\alpha$  value increases, the platform dimensions increase, and the static platform pitch angle decreases. The platform pitch angle of the upscaled platforms matches the OC4 angle of  $3.5^\circ$  at an  $\alpha$  of 0.75. Further investigation of the upscaling factor is shown in the analytical model for the semi-submersible platform (Sect. 4.5).

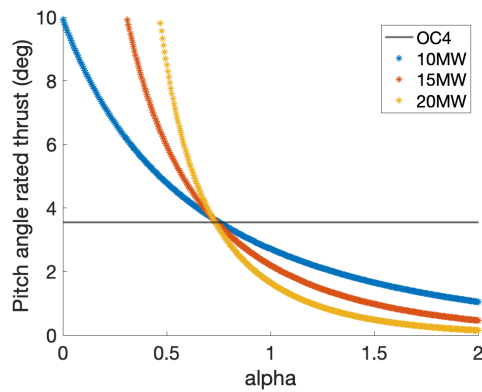


Figure 9: OC4 Platform Pitch Angle of Upscaled Systems at Rated Thrust

335

The  $T_n$  natural period of the system is also evaluated using Eq. (8), shown in Figure 10. The pitch  $T_n$  natural period is over 20 s for the entire range of  $\alpha$ , and is 24.2 s for the baseline OC4 5 MW system. Note that for the 20 MW upscaled system in the  $\alpha = 0 - 0.32$  range, the system is unstable. This is because the platform stiffness term becomes negative as the center of mass of the system is raised, with a 20 MW turbine on a platform that is too small.

340

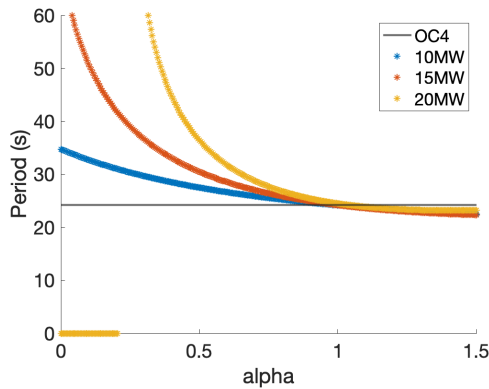


Figure 10: OC4 Natural Period of Upscaled Systems

345 The semi-submersible platform is upscaled from the OC4 design using a scaling factor of  $\alpha = 0.75$ , which is the approximate value that preserves the static platform pitch angle at rated thrust. The results are shown in Table 9. The specific power, draft, clearance between the rotor and the waterline, wall thickness, and platform pitch angle are kept constant. Please recall that the wall thickness is 4.5 cm based on the IEA design, in contrast to the 6 cm wall thickness of the OC4 design. The platform mass results would be significantly different if a larger wall thickness was used. The moment of inertia is shown for the entire system including the tower and RNA. The ratio of platform steel mass to total platform mass decreases from 27% 350 for the OC4 turbine to 18% for the 20 MW upscaled system. Fitting a curve to the mass data indicates that the platform steel mass is upscaled by  $R^{1.3}$  and the total platform mass is upscaled by  $R^{1.8}$ . The ballast mass is increasing more quickly than the steel mass, and ballast mass is significantly cheaper. The natural period of the system in pitch increases slightly as it is upscaled.

Table 9: Upscaled OC4 Table of Results

Rated Power	MW	5	10	15	20
$Sp$	$W/m^2$	401	401	401	401
Rotor radius ( $R_r$ )	m	63	89	109	126
Draft	m	20	20	20	20
$CM_{platform}$	m	-13.6	-13.1	-12.5	-12.0
$CM_{system}$	m	-10	-7.9	-6.1	-4.6
Pitch angle	deg	3.5	3.5	3.4	3.3
Total stiffness	Nm/rad	1.0E+09	2.7E+09	4.9E+09	7.6E+09
$I_{system}$	$kgm^2$	1.1E+10	3.5E+10	7.0E+10	1.2E+11
Pitch Natural period	s	24.2	26.4	27.7	28.7

- Formatted: Font: Cambria Math, 9 pt
- Formatted: Font: Cambria Math, 9 pt, Not Bold
- Formatted: Font: Cambria Math, 9 pt, Italic
- Formatted: Font: Cambria Math, 9 pt
- Formatted: Font: Cambria Math, 9 pt, Italic
- Formatted: Font: Cambria Math, 9 pt
- Formatted: Font: Cambria Math, 9 pt, Italic
- Formatted: Font: Cambria Math, 9 pt, Italic
- Formatted: Font: Cambria Math, 9 pt
- Formatted: Font: Cambria Math, 9 pt
- Formatted: Font: Cambria Math, 9 pt, Italic
- Formatted: Font: Cambria Math, 9 pt
- Formatted: Font: Cambria Math, 9 pt

Natural frequency	Hz	0.26	0.24	0.23	0.22
Steel mass	kg	3.59E+06	5.60E+06	7.30E+06	8.86E+06
Ballast mass	kg	9.70E+06	2.0E+07	3.0E+07	4.0E+07
Total platform mass	kg	1.3E+07	2.5E+07	3.7E+07	4.9E+07
Percent steel mass		27%	22%	20%	18%

Formatted: Font: Cambria Math, 9 pt

Formatted: Font: Cambria Math, 9 pt

Formatted: Font: Cambria Math, 9 pt

Formatted: Font: Cambria Math, 9 pt

Formatted: Font: Cambria Math, 9 pt

## 355 4.2 IEA Platform Upscaling Results

Figure 11 shows the static platform pitch angle at rated thrust for each  $\alpha$  increment for the IEA 15 MW upscaled platform. The platform dimensions increase with  $\alpha$ , and so the static platform pitch angle decreases. The platform pitch angle of the upscaled platforms matches the 15 MW IEA pitch value of  $4.9^\circ$  for the IEA 15 MW at  $\alpha = 0.72$ , similar to the OC4 upscaling. Further investigation of the upscaling factor is shown in the analytical model for the semi-submersible platform

360 (Sect. 4.5).

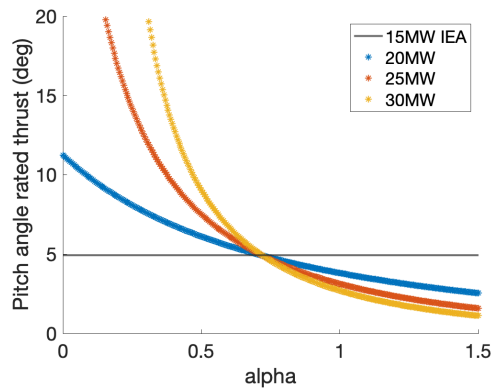


Figure 11: IEA 15 MW Platform Pitch of Upscaled Systems at Rated Thrust

The natural period is also calculated at each upscaling factor increment using Eq. (8). The pitch  $T_n$  natural-period for the 20 MW, 25 MW, and 30 MW is shown in Figure 12. The pitch  $T_n$  natural-period is over 20 s for the entire upscaling range of  $\alpha$ . The pitch  $T_n$  natural-period for the baseline IEA 15 MW platform is 28.6 s. Again, the platform becomes unstable for the 30 MW turbine in the  $\alpha = 0 - 0.18$  range because of the high center of mass of the system with the relatively small platform.

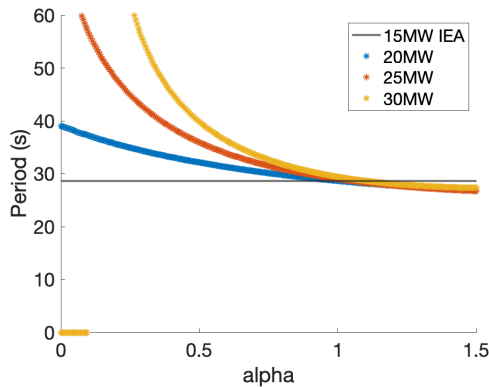


Figure 12: IEA Natural Period of Upscaled Systems

370

The semi-submersible platforms are upscaled from the IEA design using a scaling factor of  $\alpha = 0.72$  for the platform dimensions, shown in [Table 10](#). The  $332 \text{ W/m}^2$  specific power,  $4.5 \text{ cm}$  wall thickness, and  $5.9^\circ$  platform pitch angle are kept constant. Please recall that the wall thickness is  $4.5 \text{ cm}$  based on the IEA design, in contrast to the  $6 \text{ cm}$  wall thickness of the OC4 design. The platform mass results would be significantly different if a larger wall thickness was used, if required for greater structural integrity. The ratio of platform steel mass to total platform mass is reduced as the turbines are upscaled; the  $15 \text{ MW}$  IEA system has  $19\%$  steel mass, and the  $30 \text{ MW}$  IEA system has  $19\%$  steel mass compared to total platform mass including ballast. Fitting a curve to the mass data indicates that the platform steel mass is upscaled by  $R^{1.4}$  and the total platform mass is also upscaled by  $R^{2.2}$ . The  $T_n$ , natural period of the system in pitch increases slightly as it is upscaled.

375

Table 10: Upscaled IEA 15 MW Table of Results

Rated Power	MW	15	20	25	30
$S_p$	$\text{W/m}^2$	332	332	332	332
Rotor radius	m	120	138	155	170
Draft	m	20.0	22.1	24.0	25.7
$CM_{platform}$	m	-16.8	-18.6	-20.2	-21.6
$CM_{system}$	m	-5	-5.5	-5.8	-6.1
Platform pitch	deg	4.9	4.9	4.9	4.9
Total stiffness	$\text{Nm/rad}$	$3.3\text{E}+09$	$4.9\text{E}+09$	$6.8\text{E}+09$	$8.8\text{E}+09$
$I_{system}$	$\text{kgm}^2$	$5.3\text{E}+10$	$8.9\text{E}+10$	$1.4\text{E}+11$	$1.9\text{E}+11$
Pitch Natural period	s	28.6	30.3	31.9	33.2
Natural frequency	Hz	0.22	0.21	0.20	0.19

- Formatted: Font: Cambria Math, 9 pt
- Formatted: Font: Cambria Math, 9 pt, Italic
- Formatted: Font: Cambria Math, 9 pt
- Formatted: Font: Cambria Math, 9 pt
- Formatted: Font: Cambria Math, 9 pt, Italic
- Formatted: Font: Cambria Math, 9 pt
- Formatted: Font: Cambria Math, 9 pt, Italic
- Formatted: Font: Cambria Math, 9 pt
- Formatted: Font: Cambria Math, 9 pt
- Formatted: Font: Cambria Math, 9 pt, Italic
- Formatted: Font: Cambria Math, 9 pt
- Formatted: Font: Cambria Math, 9 pt

Steel mass	kg	3.5E+06	4.7E+06	6.0E+06	7.3E+06
Seawater ballast mass	kg	5.7E+06	7.7E+06	1.0E+07	1.2E+07
Fixed ballast mass	kg	9.2E+06	1.3E+07	1.6E+07	2.0E+07
Total platform mass	kg	1.8E+07	2.5E+07	3.2E+07	3.9E+07
Percent steel mass		19%	19%	19%	19%

Formatted: Font: Cambria Math, 9 pt

Formatted: Font: Cambria Math, 9 pt

Formatted: Font: Cambria Math, 9 pt

Formatted: Font: Cambria Math, 9 pt

Formatted: Font: Cambria Math, 9 pt

380

### 4.3 Case Study Discussion

Upscaling of both platforms can be compared, specifically at 20 MW. Table 11 shows the comparison between the designs, including the lower specific power and larger rotor radius of the IEA 20 MW system. The upscaled 20 MW IEA platform has a larger draft, smaller wall thickness, higher  $CM_{system}$ , and larger static platform pitch angle, whereas the upscaled 20 MW OC4 platform has a larger stiffness, moment of inertia, steel mass, and total platform mass. The pitch natural period and ratio of platform steel mass to total steel mass is similar for both designs. The 5 MW OC4 reference platform was designed in 2014 (Robertson, A., Jonkman, J., Masciola, M., Song, 2014) while the IEA 15 MW platform was designed in 2020 (Allen *et al.*, 2020), which likely explains the reduction in platform steel mass and wall thickness in the more recent design. The percentage of platform steel mass relative to the total platform mass is relatively constant at 19% for the IEA upscaling results (Table 10). In contrast, the percentage of platform steel mass relative to the total platform mass decreases for the OC4 upscaling results (Table 9). Additionally, the IEA platform steel mass scales by  $R^{1.4}$  while the OC4 platform steel mass scales by  $R^{1.32}$ . The IEA platform steel mass increases more rapidly in part because the draft is increasing while the OC4 draft is constant.

385

390

There is a 30 m gap between the blade tip and waterline for both case studies, which was kept constant during upscaling. We chose the 30 m gap because of the prevalence of this choice in practice, but this clearance will need to be explored further in future research studies. In particular, the heave motion of each upscaled turbine should be considered to ensure that there is not too large of a downward heave motion towards the waterline in any case, to ensure that the gap is not too small while considering wave height and combined platform rotational motions.

395

Table 11: Comparison of Upscaled 20 MW IEA with Upscaled 20 MW OC4 System

		Upscaled IEA 20 MW	Upscaled OC4 20 MW
$Sp$	$W/m^2$	332	401
Rotor radius	m	138	126
Draft	m	22.1	20
Wall thickness	m	0.045	0.06
$Dist_c$	m	100	84
$CM_{platform}$	m	-16.7	-11.7
$CM_{system}$	m	-5.0	-4.8

Formatted: Font: Cambria Math, 9 pt

Formatted: Font: Cambria Math, 9 pt, Italic

Formatted: Font: Cambria Math, 9 pt

Formatted: Font: Cambria Math, 9 pt

Formatted: Font: Cambria Math, 9 pt

Formatted: Font: Cambria Math, 9 pt

Formatted: Font: Cambria Math, 9 pt, Italic

Formatted: Font: Cambria Math, 9 pt

Formatted: Font: Cambria Math, 9 pt, Italic

Formatted: Font: Cambria Math, 9 pt

Formatted: Font: Cambria Math, 9 pt, Italic

Formatted: Font: Cambria Math, 9 pt

Pitch angle	deg	4.9	3.5
Total stiffness	Nm/rad	4.9E+09	7.6E+09
$I_{system}$	kg·m <sup>2</sup>	8.9E+10	1.2E+11
Pitch Natural period	s	30.3	28.7
Steel mass	kg	4.8E+06	8.9E+06
Seawater ballast mass	kg	7.8E+06	4.0E+07
Fixed ballast mass	kg	1.2E+07	0
Total platform mass	kg	2.5E+07	4.9E+07
Steel mass ratio		19%	18%

Formatted: Font: Cambria Math, 9 pt

Formatted: Font: Cambria Math, 9 pt

Formatted: Font: Cambria Math, 9 pt, Italic

Formatted: Font: Cambria Math, 9 pt

Formatted: Font: Cambria Math, 9 pt

Formatted: Font: Cambria Math, 9 pt

Formatted: Font: Cambria Math, 9 pt

Formatted: Font: Cambria Math, 9 pt

Formatted: Font: Cambria Math, 9 pt

Formatted: Font: Cambria Math, 9 pt

400

The case studies can be used to understand upscaling trends for floating platforms. Comparing four of the 5 MW OC4 systems with one upscaled 20 MW OC4 system, the total platform mass including ballast is similar, within 8%, however the platform steel mass is reduced by up to 38% for the single 20 MW turbine case. There is a lower ratio of platform steel mass to total platform mass for the upscaled platforms, primarily because the wall thickness remains constant. Rotor power scales with  $R^2$ , and so turbine power will increase more rapidly than platform steel mass as the OC4 turbines are upscaled to the  $R^{1.3}$ . Additionally, the ballast mass does increase for the upscaled systems, but the ballast cost is likely significantly lower.

405

Comparing two 15 MW IEA systems with one upscaled 30 MW IEA system, the total platform mass including ballast is similar within 6% of the mass of the 30 MW upscaled design. Additionally, the platform steel mass is 21% lower for one 30 MW system as compared with two 15 MW systems. The IEA platform mass scales to  $R^{1.4}$ , and so the platform power will scale more quickly than steel mass. This result suggests that there are advantages to continued upscaling of turbines on floating platforms, specifically when the platform draft and wall thickness are kept constant.

410

It is notable that the static pitch angle of the platform varies for each case study design. The OC4 semi-submersible static pitch angle is 3.6° and the IEA semi-submersible static pitch angle is 4.9°. Early FOWTs had a small static pitch angle to be conservative in design, but there are no absolute standards on what value of static pitch angle is acceptable.

415

The upscaling methodology is useful to identify trends for each platform type, but it should be noted that the designs are not being optimized. The original designs (OC4 and IEA 15 MW) are not optimized initially, but are designed based on expertise. The upscaled designs are also not optimized, so it is possible that other platform designs may be more stable with less platform steel mass. Optimization studies can be conducted for individual projects at specific sites, or for future research projects, but are outside the scope of this research study. Future work will also estimate levelized cost of energy (LCOE) for the upscaled turbines.

420

#### 4.4 Comparison of Platform Upscaling with Similar Studies for the OC4 Platform

The upscaled OC4 semi-submersible design can also be compared to other semi-submersible upscaling studies (George, 2014; Leimeister *et al.*, 2016; Kikuchi and Ishihara, 2019a). These upscaling studies do not seek to find platform scaling relations,

425 but instead upscale one specific design. As stated previously, Leimeister et al. (Leimeister, 2016) upscales the OC4 to a 7.5 MW and 10 MW semi-submersible, George (George, 2014) upscales OC4 to a 10 MW semi-submersible, and Kikuchi and Ishihara (Kikuchi and Ishihara, 2019a, 2019b) upscale the Fukushima FORWARD design to both a 7.5 MW and 10 MW semi-submersible. [Table 12](#) shows the 7.5 MW semi-submersible upscaling results and [Table 13](#) shows the 10 MW semi-submersible upscaling results. Both tables include the upscaled OC4 platform from this study.

**Table 12: 7.5 MW Upscaled Semi-submersible Comparison**

		Leimeister (2016)	% difference from this study	George (2014)	% difference from this study	This study
Draft	m	24.5	23%	20	0%	20
Wall thickness	m	0.078	29%	0.060	0%	0.060
<i>Rad<sub>col</sub></i>	m	7.4	5%	6.8	-3%	7.0
<i>Rad<sub>hp</sub></i>	m	14.7	5%	13.6	-3%	13.9
<i>Dist<sub>cc</sub></i>	m	61.3	5%	56.5	-3%	58.1
Static pitch angle	deg	3.7	-6%	2.4	-39%	3.9
Pitch natural period	s	34.1	34%	25.0	-2%	25.5

- Formatted: Font: Cambria Math, 9 pt
- Formatted: Font: Cambria Math, 9 pt
- Formatted: Font: Cambria Math, 9 pt
- Formatted: Font: Cambria Math, 9 pt, Italic
- Formatted: Font: Cambria Math, 9 pt
- Formatted: Font: Cambria Math, 9 pt, Italic
- Formatted: Font: Cambria Math, 9 pt
- Formatted: Font: Cambria Math, 9 pt, Italic
- Formatted: Font: Cambria Math, 9 pt
- Formatted: Font: Cambria Math, 9 pt
- Formatted: Font: Cambria Math, 9 pt

**Table 13: 10 MW Upscaled Semi-submersible Comparison**

		Leimeister (2016)	% difference from this study	George (2014)	% difference from this study	Kikuchi (2019)	% difference from this study	This study
Draft	m	25.28	26%	20.0	0%	21.3	7%	20
Wall thickness	m	0.076	27%	0.060	0%	0.060	0%	0.060
<i>Rad<sub>col</sub></i>	m	7.15	-8%	7.6	-3%	8.0	3%	7.8
<i>Rad<sub>hp</sub></i>	m	15.17	-2%	15.1	-3%	16.0	3%	15.5
<i>Dist<sub>cc</sub></i>	m	63.21	-2%	63.0	-3%	54.3	-16%	64.8
Static pitch angle	deg	4.8	26%	3.1	-18%	4.5	20%	3.8
Pitch natural period	s	33.2	26%	28.0	6%	26.0	-1%	26.4

- Formatted: Font: Cambria Math, 9 pt
- Formatted: Font: Cambria Math, 9 pt
- Formatted: Font: Cambria Math, 9 pt, Italic
- Formatted: Font: Cambria Math, 9 pt
- Formatted: Font: Cambria Math, 9 pt, Italic
- Formatted: Font: Cambria Math, 9 pt
- Formatted: Font: Cambria Math, 9 pt, Italic
- Formatted: Font: Cambria Math, 9 pt
- Formatted: Font: Cambria Math, 9 pt
- Formatted: Font: Cambria Math, 9 pt
- Formatted: Font: Cambria Math, 9 pt

435 All studies upscale the platform based on the increase in power rating. George (George, 2014) and Kikuchi and Ishihara (Kikuchi and Ishihara, 2019a, 2019b) limit certain dimensions such as draft and platform wall thickness, and all check criteria to ensure the design meets natural period and static pitch angle requirements. Each of these studies use the ~~RNA/RNA~~ mass upscaling ratio in order to set the upscaling factor for the platform. Leimeister ~~et al.~~ (Leimeister, 2016) upscales the platform dimensions using a scaling factor of 1.264 ~~for the 10 MW design, and then scaling is adjusted separately for the main column and upper columns. This is the starting point, and then scaling is adjusted for the main column.~~ George (George, 2014) uses a scaling factor of 1.26 ~~for the 10 MW design,~~ based on the mass scaling. For the 10 MW upscaling results, the other three studies all have a similar or smaller spread between the outer columns as compared with this study.

440 The platform dimensions of this study are within 3% of the results for George (George, 2014) for all platform dimensions shown. The only notable difference is that the calculated static pitch angle is lower for George (George, 2014) even though the platform is slightly smaller than the one modeled in this study. The Leimeister et al. (Leimeister *et al.*, 2016) study is the only one that increases both the draft and wall thickness with upscaling. Additionally, the platform pitch natural period is 34% larger for Leimeister et al. (Leimeister *et al.*, 2016) due to the larger platform dimensions. Finally, the Kikuchi and Ishihara (Kikuchi and Ishihara, 2019a, 2019b) study has a 16% smaller distance between the outer columns, which causes an increase in the static pitch angle.

450 Overall, the Leimeister et al. (Leimeister *et al.*, 2016) study is the most conservative, the George (George, 2014) study is the most similar to the method proposed here, and the Kikuchi and Ishihara (Kikuchi and Ishihara, 2019a, 2019b) study increases the draft but reduces the spread between columns. The spread between the columns provides the largest contribution to stability for the semi-submersible platform type, so this reduction in column spread may have drawbacks.

455 This proposed upscaling method differs from the other methods in that there is one platform dimension upscaling factor identified, which can be used in Eq. (1) to upscale any semi-submersible platform. Please note that the scaling relations are only valid for a similar semi-submersible design with three outer columns forming a triangle and one central turbine. This is in contrast to the other studies which upscale one specific case study through a variety of methods that include some trial and error, and do not result in a scaling factor.

#### 4.5 Analytical Model for Semi-submersible Platform Upscaling

460 There are classical analytical scaling laws for wind turbines (Manwell, McGowan and Rogers, 2009), but the scaling laws for FOWT platforms are not fully understood. The results from the case studies can be used to develop analytical upscaling relations for the semi-submersible platforms. For the static pitch angle to match the original semi-submersible design, an upscaling factor of approximately  $\alpha = 0.72 - 0.75$  was found for both the OC4 5 MW and IEA 15 MW designs. Additionally, the platform steel mass scales with  $R^{1.3} - R^{1.4}$  when the wall thickness is kept constant. Platform mass, but would scale to a greater ratio if the wall thickness increases proportionally with  $R$  (Sieros *et al.*, 2012). Thus, the upscaling is more advantageous in terms of platform steel mass when the wall thickness is kept constant. However, increasing the platform wall thickness may be required for the structural integrity of the FOWT system, and this is an important area of future research.



These results have been determined using hydrodynamic models and an iterative method, but fundamental equations for the static pitch when upscaling can also be derived analytically. The static pitch equation is shown in Eq. (11), which is an expanded version of Eq. (4).

$$\theta_p = \frac{M_{aero}}{\rho g W_{55} + \rho g V_{disp}(B - CM_{system})} \quad (11)$$

The numerator is the aerodynamic moment on the platform at rated wind speed, which is the thrust of the wind turbine multiplied by the distance between the rotor hub and the center of mass of the system. The denominator of the equation is the platform stiffness  $C_{55}^{hydrostatics}$ . The mooring stiffness is neglected in these calculations; Section 4.3 addresses this assumption with a sensitivity study. The platform stiffness includes two terms, one is based on buoyancy ( $V_{disp}(B - CM_{system})$ ) and the other on waterplane area ( $W_{55}$ ). The waterplane area term provides the dominant stability for semi-submersible platforms, contributing 94% for the 15 MW IEA. Literature shows that the buoyancy term is always small for semi-submersible platforms, and other research studies have neglected the buoyancy term in the stiffness equation for semi-submersible upscaling (Kikuchi and Ishihara, 2019a). For both the OC4 and IEA semi-submersible platforms, the buoyancy term is actually destabilizing because the turbine and tower mass raise the  $CM_{system}$  above position  $B$ . Eq. (11) can be simplified to Eq. (12) by neglecting the buoyancy term and only considering the waterplane area term in the denominator.

$$\theta_{p,s} = \left[ \frac{Th \times h}{\rho g W_{55}} \right]_{original} = \left[ \frac{Th \times h}{\rho g W_{55}} \right]_{new} \quad (12)$$

There is aerodynamic similarity between the original and upscaled turbine with constant density of air, thrust coefficient, and rated wind speed. The thrust is  $Th$  and  $h$  is the distance between the hub and the  $CM_{system}$ . For simplicity, the hub height is used and the distance from the  $CM_{system}$  and the waterline is neglected. The hub height is 90% of the total distance for the OC4 and 98% for the IEA 15 MW designs. Additionally, the hub height is defined as 1.25 times the rotor radius in this model. This gives the 30 m clearance for the 15 MW IEA turbine and increases the clearance for larger turbines. The second moment area of the waterplane for the IEA semi-submersible is calculated using Eq. (13), which is also shown in a simplified version in Eq. (14).

$$W_{55} = \frac{\pi}{4} [Rad_{cent}^4 + 3(Rad_{col})^4] + 2\pi(Rad_{col})^2(8.28 * \sin 60 * Rad_{col})^2 \quad (13)$$

$$W_{55} = \frac{\pi}{4} (Rad_{cent})^4 + \left(\frac{3\pi}{4}\right) (138)(Rad_{col})^4 \quad (14)$$

Calculating  $W_{55}$  for the 15MW IEA platform, the first term (central column) is 0.1% of the total and the second term (three outer columns) is 99.9%, indicating that nearly all of the stability comes from the three outer columns. Thus, the first term is neglected and only the column radius term is considered. The thrust and hub height equations are shown in Eq. (15). The rotor diameter is defined as  $\phi$ , with  $\phi_{original}$  as the original rotor diameter and  $\phi_{new}$  as the rotor diameter of the upscaled turbine.

$$\frac{\left(\frac{1}{2}\rho\alpha\pi\left(\frac{\phi_{original}}{2}\right)^2 C_T u^2\right)\left(1.25\left(\frac{\phi_{original}}{2}\right)\right)}{103.6\pi(Rad_{col,original})^4} = \frac{\left(\frac{1}{2}\rho\alpha\pi\left(\frac{\phi_{NEW}}{2}\right)^2 C_T u^2\right)\left(1.25\left(\frac{\phi_{NEW}}{2}\right)\right)}{103.6\pi(Rad_{col,NEW})^4} \quad (15)$$

Note that any semi-submersible with three outer columns [forming an equilateral triangle](#) would reduce to the same equation, because the coefficient terms cancel out. Eq. (15) can be further simplified to only include the column radius and rotor diameter

Eq. (16).

$$\frac{(\phi_{original})^3}{(Rad_{col\_original})^4} = \frac{(\phi_{NEW})^3}{(Rad_{col\_NEW})^4} \quad (16)$$

This scaling relation for the semi-submersible platform can determine the column radius needed for an upscaled semi-submersible platform based on the original column radius, and the diameter of the original and upscaled turbines. Eq. (17) is in a similar format to the generic scaling relation shown in Eq. (1). The scaling factor between the upscaled column radius and the original column radius is  $\alpha = 0.75$ , which is very similar to the upscaling factor of  $\alpha = 0.72-0.75$  that was found for the semi-submersible case studies. Thus, the analytical formulation recovers the same upscaling factor as the more complex hydrodynamic model.

$$Rad_{col\_NEW} = (Rad_{col\_original}) * \left[ \frac{\phi_{NEW}}{\phi_{original}} \right]^{3/4} \quad (17)$$

This relation is similar to the square-cube law of blade upscaling, except that it shows that platform upscaling is likely to be advantageous because platform stiffness scales faster than wind turbine overturning moment. The upscaled column radius scales at  $\alpha = 0.75$  because the overturning moment from rated thrust is proportional to the diameter cubed, and the stiffness is dominated by the column radius to the fourth power. This only defines column radius and column spread, but all parameters can be upscaled by the same  $\alpha$  of 0.75 for a semi-submersible upscaled design. Additionally, if it is assumed that all semi-submersible platform dimensions increase, including wall thickness and draft, the platform steel mass increases by a factor of 2.25 in Eq. (18). However, if the platform wall thickness is kept constant, as it was in the case studies, the platform steel mass increases by a factor of 1.5. If multiple small FOWTs were used instead of upscaling, the steel mass would scale as  $R^2$  [because the power would scale with the rotor swept area and the system mass would scale proportionally](#) (Manwell, McGowan and Rogers, 2009; Jamieson, 2018).

$$M_{platform\_NEW} = (M_{platform\_original}) * \left[ \frac{\phi_{NEW}}{\phi_{original}} \right]^{1.5} \quad (18)$$

## 4.6 Sensitivity Studies

The results presented above rely on a variety of assumptions, which are now assessed using parameter sensitivity studies.

### 4.6.1 Mooring Line Sensitivity

This research assumes that the stiffness contributions from the mooring lines can be neglected for the first-order platform pitch angle calculations. A mooring line sensitivity study is conducted to evaluate the contribution of mooring line stiffness to platform pitch motion. The study uses the OC4 system using OpenFAST and evaluates the natural period of the system when the mooring line stiffness is reduced. The published  $T_n$  [natural period](#) of the system is 27 s. OpenFAST is run with the tower degrees of freedom off, and the pitch  $T_n$  [natural period](#) is calculated using a free decay test ([Figure 13](#)[Figure 13](#)-[Figure 14](#)[Figure](#)

14). The mooring line stiffness ( $EA$ ) is then decreased from the original stiffness value to a stiffness that is one-eighth of the original value. The  $T_n$  natural period is calculated for each simulation to determine the impact on the system dynamics.

530 Table 14 shows that reducing the mooring line stiffness by a factor of eight reduces the pitch  $T_n$  natural period of the system by less than 1%.

Table 14: Pitch Natural Period of OC4 with Reduced Mooring Line Stiffness

$EA$ (MN)	$T_n$ (s)	502.4 (/1.5)	376.8 (/2)	188.4 (/4)	94.2 (/8)
753.6	25.535	25.5625	25.590	25.645	25.740
502.4 (/1.5)	25.5625				
376.8 (/2)	25.590				
188.4 (/4)	25.645				
94.2 (/8)	25.740				

Formatted: Font: Cambria Math, 9 pt, Not Bold, Italic

Formatted: Font: Cambria Math, 9 pt, Not Bold

Formatted: Font: Not Italic

Formatted Table

Formatted: Font: Cambria Math, 9 pt

Formatted: Font: Cambria Math, 9 pt

Formatted: Font: Cambria Math, 9 pt

Formatted: Font: Cambria Math, 9 pt

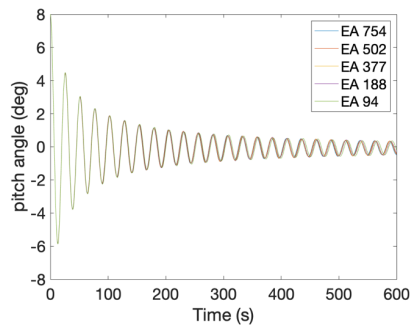


Figure 13: Free Decay Test for OC4

535

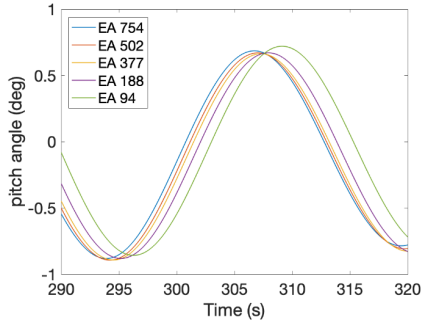


Figure 14: Free Decay Test of OC4 for 30 second Interval

The static pitch angle at rated thrust can also be evaluated in OpenFAST while decreasing the mooring line stiffness. OpenFAST is run for the OC4 system at steady, rated wind speed (Figure 15). Table 15 shows that when the mooring line stiffness is reduced by a factor of eight, the static pitch angle is increased by less than 1%. Thus, while mooring design may change as platform size increases, these results indicate that the mooring stiffness has negligible impact on the platform dynamics, and so can be ignored in upscaling studies. Further analysis of mooring line behavior is therefore outside the scope of this research.

Table 15: Static Pitch Angle of OC4 with Mooring Stiffness

EA (MN)	Pitch angle (deg)	502.4 (/1.5)	376.8 (/2)	188.4 (/4)	94.2 (/8)
753.6	3.2592	3.2618	3.2636	3.2729	3.2809
502.4 (/1.5)	3.2618				
376.8 (/2)	3.2636				
188.4 (/4)	3.2729				
94.2 (/8)	3.2809				

Formatted: Font: Cambria Math, 9 pt, Italic

Formatted Table

Formatted: Font: Cambria Math, 9 pt

Formatted: Font: Cambria Math, 9 pt

Formatted: Font: Cambria Math, 9 pt

Formatted: Font: Cambria Math, 9 pt

Formatted: Font: Cambria Math, 9 pt

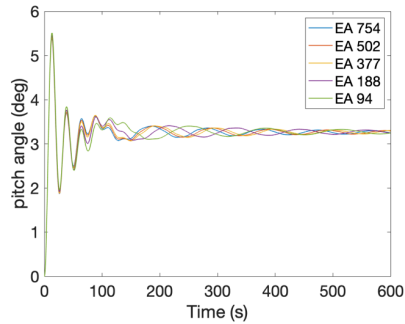


Figure 15: Static Pitch of OC4 at Rated Thrust with Mooring Line Stiffness

#### 4.6.2 Rotor Nacelle Assembly Mass Sensitivity

The upscaling case studies are conducted with an assumption about the mass scaling of the rotor nacelle assembly (*RNA*). Classical upscaling uses  $R^3$  scaling of *RNA* mass, while scaling based on data results in  $R^{2.2}$  scaling approximately. In addition to the impact on turbine mass, the change in *RNA* mass scaling also impacts the FOWT platform design, mass, and cost. While some researchers have focused on reducing turbine mass to reduce the size and cost of the platform (Jacob C. Ward, Andrew J. Goupee, Anthony M. Viselli, 2021), it is still unclear if *RNA* mass reduction is a major design driver for FOWT design.

An *RNA* mass sensitivity study is conducted for the IEA 15 MW wind turbine. The *RNA* mass is reduced to 50% of the original mass, while the tower mass remains constant. As the *RNA* mass decreases, the platform size is reduced so that the platform pitch angle at rated thrust remained constant. Table 16 shows the results of the *RNA* mass sensitivity study for the 15 MW IEA semi-submersible.

Table 16: RNA Mass Sensitivity Results for IEA 15 MW

<i>RNA</i> mass reduction	<i>RNA</i> mass	Platform pitch angle	<i>CM</i>	Total stiffness	Steel mass	Steel mass reduction	Total platform mass	Platform mass reduction
▲	kg	deg	m	Nm/rad	kg	%	kg	%
original	1.02E+06	7.8	-2.7	2.77E+09	3.88E+06		1.84E+07	
5%	9.66E+05	7.6	-3.1	2.86E+09	3.88E+06	0%	1.85E+07	0%
15%	8.64E+05	7.8	-3.4	2.81E+09	3.81E+06	-2%	1.79E+07	-3%
29%	7.19E+05	7.7	-4.1	2.85E+09	3.73E+06	-4%	1.75E+07	-5%
42%	5.87E+05	7.7	-4.8	2.87E+09	3.65E+06	-6%	1.70E+07	-7%
50%	5.09E+05	7.9	-5.1	2.81E+09	3.58E+06	-8%	1.65E+07	-10%

Formatted: Font: Not Italic

Formatted: Font: Not Italic

Formatted: Font: Not Italic

Formatted: Font: Not Italic

Formatted: Font: Not Italic

Formatted: Font: Not Italic

Formatted: Font: Not Italic

Formatted: Font: Cambria Math, 9 pt, Not Bold

Formatted: Font: Cambria Math, 9 pt, Not Bold, Italic

Formatted: Font: Cambria Math, 9 pt, Not Bold

Formatted: Font: Cambria Math, 9 pt, Not Bold

Formatted: Font: Cambria Math, 9 pt

Formatted: Font: Cambria Math, 9 pt

Formatted: Font: Cambria Math, 9 pt

Formatted: Font: Cambria Math, 9 pt

Formatted: Font: Cambria Math, 9 pt

Formatted: Font: Cambria Math, 9 pt

560

The results show that the  $CM_{system}$  lowers with the reduced ~~RNA~~ mass. A smaller platform is also needed to support the smaller ~~RNA~~ mass (because of the lower center of mass). The platform steel mass is reduced by 8% (300,000 kg) when the ~~RNA~~ mass is reduced by 50% (510,000 kg) and the total platform mass including ballast is reduced by 10%. The waterplane area component of the platform stiffness is stabilizing, while the contribution from the center of mass is destabilizing; thus, when the ~~RNA~~ mass is reduced by 50%, the destabilizing stiffness term is reduced by 35%. The RNA mass impacts the upscaling results, but the sensitivity study shows that it is reasonable to assume the constant  $R^{2.2}$  RNA upscaling within the scope of this study.

565

#### 4.7 Discussion of Results

570

The results are useful for upscaling a semi-submersible platform to a larger size, especially as a preliminary design analysis before a more detailed design process. These results are applicable for a semi-submersible platform with three outer columns forming a triangle and the turbine mounted in the center. There are a wide variety of other FOWT designs that would be interesting to study, including more unique semi-submersible designs (e.g., four outer columns forming a square with one central column or the turbine mounted on one outer column instead of the central column), spar designs, and tension-leg platform designs. If a researcher wants to upscale a ~~three-column~~ triangular semi-submersible platform with three outer columns and the turbine centrally mounted to a size of 6 - 30 MW, this method can give a good estimate of the platform dimensions and mass based on an original design and larger wind turbine parameters.

575

The limitations of this method include several the simplifications assumed in order made to identify the upscaling trends. The dynamics of the FOWT system needs further evaluation, including second order effects. However, this study chooses to focus exclusively on the platform pitch motion during rated thrust, as this has been shown to be thean important primary-load case. Additionally, environmental conditions such as wind-wave misalignment are not considered in this case. The purpose of this research study is to identify the upscaling trends using the simplified assumptions, and leave further evaluation of detailed design to future research studies. The benefit of this method is identifying an upscaled design with little computational time and expense.

580

Future work should validate the upscaled FOWT designs using OpenFAST, which involves creating a turbine and platform model for each upscaled design. Additionally, future research is needed of to assess the structural integrity of the FOWT platform assuming constant wall thickness with upscaling. The constant clearance assumption between the blade tip and waterline wouldcan also be benefieialassessed, in addition to checking the heave motions of future researh studies to ensure that heave motions they are within a reasonable range for platform motions. A better understanding of the upscaled designs in extreme wind and wave conditions can further the knowledge of platform upscaling. An additional area of future work is to conduct cost of energy analysis, in order to gain insight into how turbine and platform scaling impact the system economics. Upscaling the platform with a constant wall thickness causes the platform steel mass to increase with a factor of approximately  $R^{1.5}$ , suggesting that larger turbines may be advantageous. But a more nuanced and detaidetailed analysis is needed, which

585

590

Formatted: Normal

includes balance of system costs and estimates on annual energy production, to assess the likely impact of continued upscaling of FOWTs.

Formatted: Font color: Auto

## 5 Conclusion

Floating offshore wind turbines are being developed to harness energy in windy, deep-water sites. While individual floating platform designs can be optimized for a specific site, this research provides fundamental insight that can guide technology development by creating a generalized methodology for semi-submersible platform upscaling. This work has resulted in an upscaling factor for a triangular three-column semi-submersible platforms with three outer columns and a centrally mounted turbine. The upscaling factors for dimensions and mass are that is comparable to the classical turbine scaling relations (Manwell, McGowan and Rogers, 2009).

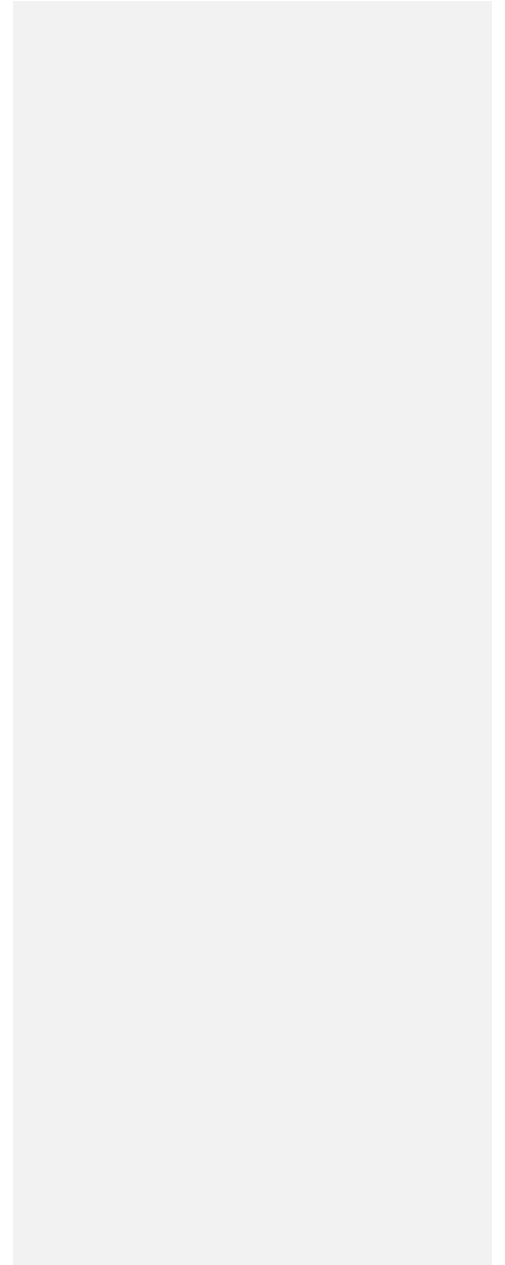
The numerical method used in the methodology was validated using OpenFAST. The upscaled platform results are closest to those of George (George, 2014), but the results do differ from other similar research studies (George, 2014; Leimeister *et al.*, 2016; Kikuchi and Ishihara, 2019a; Ju *et al.*, 2020). Additionally, this study differs from the generic semi-submersible scaling study conducted by Wu and Kim (Wu and Kim, 2021), because their method is an iterative approach to find the column radius and spread for a semi-submersible, and there is no scaling factor provided.

Two upscaling case studies are evaluated: the OC4 semi-submersible turbine is upscaled from 5 MW to 20 MW and the IEA 15 MW semi-submersible turbine is upscaled from 15 MW to 30 MW. The semi-submersible scale factor for both case studies is approximately  $\alpha = 0.75$ , using both numerical and analytical methods. These relations can be used to quickly estimate the platform dimensions for a larger turbine rotor. Additionally, the analytical solution shows that platform steel mass increases with  $R^{1.5}$  when platform wall thickness is kept constant using the upscaling method, and  $R^2$  when multiple, smaller FOWTs are used instead of upscaling. Thus, platform upscaling is shown to be advantageous regarding platform steel mass cost savings as compared to installing multiple, smaller FOWT systems. Having fewer, larger FOWT systems will improve other aspects of offshore wind farms, such as fewer turbines to install and maintain in difficult to access ocean environments. However, there will likely need to be an upper limit to FOWT upscaling, likely related to the increased stresses due to blade weight that continue to scale linearly with rotor radius.

~~Future work should validate the upscaled FOWT designs using OpenFAST, which involves creating a turbine and platform model for each upscaled design. A better understanding of the upscaled designs in extreme wind and wave conditions can further the knowledge of platform upscaling. An additional area of future work is to conduct cost of energy analysis, in order to gain insight into how turbine and platform scaling impact the system economics. Upscaling the platform with a constant wall thickness causes the platform steel mass to increase with a factor of approximately  $R^{1.5}$ , suggesting that larger turbines may be advantageous. But a more nuanced and detail analysis is needed, which includes balance of system costs and estimates on annual energy production, to assess the likely impact of continued upscaling of FOWTs. The upscaling of FOWT systems~~

625 is already taking place in industry, and better understanding of platform scaling can give key insight into research and industry development.

|





## References

- 630 Ågotnes, A. *et al.* (2013) *Deep water: The next step for offshore wind*. Brussels, Belgium: The European Wind Energy Association (EWEA). Available at: [https://www.researchgate.net/publication/257553940\\_Deep\\_Water\\_The\\_next\\_step\\_for\\_offshore\\_wind\\_energy\\_A\\_report\\_by\\_the\\_European\\_Wind\\_Energy\\_Association](https://www.researchgate.net/publication/257553940_Deep_Water_The_next_step_for_offshore_wind_energy_A_report_by_the_European_Wind_Energy_Association).
- Allen, C. *et al.* (2020) *Definition of the UMaine VolturnUS-S Reference Platform Developed for the IEA 15MW Wind Turbine*. Golden, CO. Available at: <https://www.nrel.gov/docs/fy20osti/76773.pdf>.
- 635 Ashuri, T. (2012) *Beyond Classical Upscaling : Integrated Aeroservoelastic Design and Optimization of Large Offshore Wind Turbines*. Delft University of Technology. doi: 10.4233/uuid:d10726c1-693c-408e-8505-dfca1810a59a.
- Beaubouef, B. (2020) *WindFloat Atlantic represents major offshore wind milestone, Offshore*. Available at: <https://www.offshore-mag.com/renewable-energy/article/14188688/windfloat-atlantic-represents-major-offshore-wind-milestone>.
- 640 Beiter, P. *et al.* (2016) "A Spatial-Economic Cost- Reduction Pathway Analysis for U.S. Offshore Wind Energy Development from 2015–2030," *National Renewable Energy Laboratory (NREL)*, (September), p. 214.
- Beiter, P. *et al.* (2020) *The Cost of Floating Offshore Wind Energy in California Between 2019 and 2032*. Golden, CO. Available at: <https://www.nrel.gov/docs/fy21osti/77384.pdf>.
- Buljan, A. (2023) *GE Developing 18 MW Haliade-X Offshore Wind Turbine, offshoreWind.biz*. Available at: <https://www.offshorewind.biz/2023/03/14/ge-developing-18-mw-haliade-x-offshore-wind-turbine/> (Accessed: May 11, 2023).
- 645 California Energy Commission (2021) *Offshore Renewable Energy*. Available at: <https://www.energy.ca.gov/programs-and-topics/topics/renewable-energy/offshore-renewable-energy>.
- Conversation, T. (2021) *California is planning floating wind farms offshore to boost its power supply - here's how they work*. Available at: <https://theconversation.com/california-is-planning-floating-wind-farms-offshore-to-boost-its-power-supply-heres-how-they-work-163419>.
- 650 Delhommeau, G. (1993) *Numerical Simulation of Hydrodynamics: Ships and Offshore Structures: Seakeeping codes AQUADYN and AQUAPLUS*. Nantes, France.
- Det Norske Veritas Germanischer Lloyd (2017) "DNVGL-RP-C205: Environmental Conditions and Environmental Loads,"
- 655 *DNV GL Recommended Practice*, (DNVGL-RP-C205), pp. 1–259.
- Duarte, T. M., Sarmiento, A. J. and Jonkman, J. (2014) "Effects of second-order hydrodynamic forces on floating offshore wind turbines," *32nd ASME Wind Energy Symposium*, (April). doi: 10.2514/6.2014-0361.
- Durakovic, A. (2021) *Largest Floating Offshore Wind Farm Stands Complete, offshoreWind.biz*. Available at: <https://www.offshorewind.biz/2021/08/24/largest-floating-offshore-wind-farm-stands-complete/>.
- 660 Equinor (2021) *Hywind Scotland*. Available at: <https://www.equinor.com/en/what-we-do/floating-wind/hywind->

- scotland.html.
- Fukushima Offshore Wind Consortium (no date) *Fukushima Floating Offshore Wind Farm Demonstration Project*. Available at: <http://www.fukushima-forward.jp/english/>.
- Gaertner, E. *et al.* (2020) *Definition of the International Energy Agency 15-Megawatt Offshore Reference Wind Turbine*. Golden, CO. Available at: <https://www.nrel.gov/docs/fy20osti/75698.pdf>.
- 665 GE Renewable Energy (2023) *Haliade-X Offshore wind turbine*. Available at: <https://www.ge.com/renewableenergy/wind-energy/offshore-wind/haliade-x-offshore-turbine>.
- George, J. (2014) *WindFloat design for different turbine sizes*. Instituto Superior Tecnico.
- Jacob C. Ward, Andrew J. Goupee, Anthony M. Viselli, H. J. D. (2021) “Experimental investigation into the dynamic behavior of a floating offshore wind turbine stabilized via a suspended counterweight,” *Ocean Engineering*, 228.
- 670 Jamieson, P. (2018) “Upscaling of Wind Turbine Systems,” in *Innovation in Wind Turbine Design*. second. John Wiley & Sons, Ltd., pp. 97–126.
- Jonkman, J. M., Matha, D. (2011) “Dynamics of offshore floating wind turbines-analysis of three concepts,” *Wind Energy*, (14), pp. 557–569.
- 675 Jonkman, J. *et al.* (2009) *Definition of a 5-MW reference wind turbine for offshore system development*. Golden, CO. Available at: <https://www.nrel.gov/docs/fy09osti/38060.pdf>.
- Jonkman, J. (2019) “OpenFAST : An Open-Source Tool for Wind Turbine Physics-Based Engineering Modeling,” in *North American Wind Energy Academy (NAWEA)/WindTech 2019*. Amherst, MA.
- Jonkman, J. M. (2007) *Dynamics modeling and loads analysis of an offshore floating wind turbine*. Golden, CO: National Renewable Energy Laboratory.
- 680 Jonkman, J. M. and Buhl, M. L. (2005) *FAST User’s Guide*. Golden, CO. doi: 10.2172/15020796.
- Ju, S. *et al.* (2020) “Study of optimal large-scale offshore wind turbines,” *Renewable Energy*, (154), pp. 161–174.
- Karimirad, M. (2014) *Offshore Energy Structures, Springer*. Springer International Publishing. doi: 10.1007/978-3-319-12175-8.
- 685 Kikuchi, Y. and Ishihara, T. (2019a) “Upscaling and levelized cost of energy for offshore wind turbines supported by semi-submersible floating platforms,” *Journal of Physics: Conference Series*, 1356(1), pp. 0–12. doi: 10.1088/1742-6596/1356/1/012033.
- Kikuchi, Y. and Ishihara, T. (2019b) “Upscaling and levelized cost of energy for offshore wind turbines supported by semi-submersible floating platforms,” in *EERE DeepWind Conference*. doi: 10.1088/1742-6596/1356/1/012033.
- 690 Kikuchi, Y. and Ishihara, T. (2020) “Comparison of dynamic response and levelized cost of energy on three platform concepts of floating offshore wind turbine systems,” *Journal of Physics: Conference Series*, 1452(1). doi: 10.1088/1742-6596/1452/1/012035.
- Leimeister, M. (2016) *Rational Upscaling and Modelling of a Semi-Submersible Floating Offshore Wind Turbine, European Wind Energy Master: Offshore Engineering Track*.

- 695 Leimeister, M. *et al.* (2016) “Rational Upscaling of a Semi-submersible Floating Platform Supporting a Wind Turbine,” *Energy Procedia*. The Author(s), 94(January), pp. 434–442. doi: 10.1016/j.egypro.2016.09.212.
- Manwell, J. F., McGowan, J. G. and Rogers, A. L. (2009) *Wind Energy Explained Theory, Design, and Application*. Second Edi, Wiley. Second Edi. Chichester, West Sussex, United Kingdom: John Wiley & Sons, Ltd. doi: 10.1016/B978-0-12-804448-3/00004-9.
- 700 Musial, W. *et al.* (2016) *2016 Offshore Wind Energy Resource Assessment for the United States*. Golden, CO. Available at: <https://www.nrel.gov/docs/fy16osti/66599.pdf>.
- Musial, W. *et al.* (2022) *Offshore Wind Market Report: 2022 Edition*. Available at: <https://www.osti.gov/servlets/purl/1883382/>.
- National Renewable Energy Laboratory (2020) *OpenFAST Documentation Release v2.5.0*. Golden, CO. Available at: <http://openfast.readthedocs.io/en/master/source/user/beamdyn/introduction.html>.
- 705 Principle Power (no date) *WindFloat*. Available at: <https://www.principlepowerinc.com/en/windfloat>.
- Robertson, A., Jonkman, J., Masciola, M., Song, H. (2014) *Definition of the Semisubmersible Floating System for Phase II of OC4*. Golden, CO. Available at: <https://www.nrel.gov/docs/fy14osti/60601.pdf>.
- Sebastian, T. and Lackner, M. (2012) “Analysis of the induction and wake evolution of an offshore floating wind turbine,” *Energies*, 5(4), pp. 968–1000. doi: 10.3390/en5040968.
- 710 Shields, M. *et al.* (2021) “Impacts of turbine and plant upsizing on the levelized cost of energy for offshore wind,” *Applied Energy*. Elsevier Ltd, 298, p. 117189. doi: 10.1016/j.apenergy.2021.117189.
- Siemens Gamesa (2020) *SG 14-222 DD*. Available at: <https://www.siemensgamesa.com/en-int/products-and-services/offshore/wind-turbine-sg-14-222-dd>.
- 715 Sieros, G. *et al.* (2012) “Upscaling wind turbines: theoretical and practical aspects and their impact on the cost of energy,” *Wind Energy*, 15(1), pp. 3–17. doi: 10.1002/we.527.
- Skaare, B. *et al.* (2006) “Integrated dynamic analysis of floating offshore wind turbines,” *European Wind Energy Conference and Exhibition 2006, EWEC 2006*, 3(January), pp. 1834–1842.
- Souza, C. E. S. de and Bachynski-Polić, E. E. (2022) “Design, structural modeling, control, and performance of 20 MW spar floating wind turbines,” *Marine Structures*. Elsevier Ltd, 84(March 2022). doi: 10.1016/j.marstruc.2022.103182.
- 720 Speer, B., Keyser, D. and Tegen, S. (2016) *Floating Offshore Wind in California: Gross Potential for Jobs and Economic Impacts from Two Future Scenarios*. Golden, CO. Available at: <https://www.nrel.gov/docs/fy16osti/65352.pdf>.
- The University of Maine (2021) *Advanced Structures and Composites Center*. Available at: <https://composites.umaine.edu/offshorewind/>.
- 725 Thiagarajan, K. P. and Dagher, H. J. (2014) “A Review of Floating Platform Concepts for Offshore Wind Energy Generation,” *Journal of Offshore Mechanics and Arctic Engineering*, 136, pp. 1–6.
- Thresher, R., Robinson, M. and Veers, P. (2008) *Wind Energy Technology : Current Status and R & D Future*. Golden, CO. Available at: <http://www.nrel.gov/docs/fy08osti/43374.pdf>.

TU Delft (2006) "Chapter 6 Rigid Body Dynamics," in, pp. 173–176.

730 Vestas (2023) *V236-15.0MW*. Available at: <https://us.vestas.com/en-us/products/offshore/V236-15MW>.

Wang, C. M. *et al.* (2010) "Research on floating wind turbines: A literature survey," *IES Journal Part A: Civil and Structural Engineering*, 3(4), pp. 267–277. doi: 10.1080/19373260.2010.517395.

Wu, J. and Kim, M. H. (2021) "Generic upscaling methodology of a floating offshore wind turbine," *Energies*, 14(24), pp. 1–14. doi: 10.3390/en14248490.

735 Yao, S. *et al.* (2021) "Aero-structural design and optimization of 50 MW wind turbine with over 250-m blades," *Wind Engineering*. doi: 10.1177/0309524X211027355.

Yoshimoto, H. *et al.* (2013) "Development of floating offshore substation and wind turbine for Fukushima FORWARD," in *Proceedings of the International Symposium on Marine and Offshore Renewable Energy*, pp. 1–9.

740

Formatted: French